Int. J Solids Structures Vol 23, No 2, pp 267–285, 1987
Printed in Great Britain

0020–7683/87 $3.00 + .00
Pergamon Journals Ltd

ON THE LONGITUDINAL HARMONIC MOTION OF AN ELASTIC BAR EMBEDDED IN AN ELASTIC HALF-SPACE

R. K. N. D. RAJAPAKSE and A. H. SHAH
Department of Civil Engineering, University of Manitoba, Winnipeg, Canada R3T 2N2

(*Received* 23 *October* 1985; *in revised form* 26 *March* 1986)

Abstract—The present study is concerned with the motion of a long cylindrical elastic bar which is partially embedded in a homogeneous elastic half-space and subjected to a harmonic axial load. Initially Green's functions corresponding to axisymmetric harmonic ring loads are derived and presented explicitly. It is found that the direct extension of elastostatic solution schemes to solve elastodynamic problems may lead to erroneous solutions due to the inability of these algorithms to properly account for inertia effects. Some discrepancies in existing solutions with respect to the inertia component of the bar are shown. An efficient solution scheme, based on Lagrange's equation of motion and a discretization technique, is presented to solve the title problem. Numerical results are presented to illustrate the influence of bar flexibility, mass density, geometry, and frequency of excitation on the axial impedance of the system.

INTRODUCTION

The study of finite cylindrical elastic inclusions which are partially embedded in an elastic half-space and subjected to a symmetric harmonic axial load (Fig. 1), has great importance in several branches of engineering. The fundamental work in this area is due to Muki and Sternberg[1], who considered the diffusion of a static axial load from an infinitely long circular elastic bar into the surrounding infinite elastic medium. This exact analytical study provided the basis for a later study by Muki and Sternberg[2], where an analytical formulation based on one-dimensional continuum for the bar was presented to investigate the elastostatic axial load transfer from a long cylindrical elastic bar into the surrounding elastic half-space.

Keer and Freeman[3] considered the transfer of a static torque from an infinite cylindrical bar into the surrounding half-space. Niumpradit and Karasudhi[4] and Karasudhi *et al.*[5, 6] have extended the scheme of Ref. [2] to quasi-static axial load transfer, torque transfer problems, and also to investigate the effect of a modified compatibility condition. It is considered that an exact analytical formulation of the problem of a finite elastic bar involves several fundamental difficulties. However, elegant analytical formulations based on coupled singular integral equations exist for elastostatic axisymmetric problems of a finite rigid bar. These are due to Luk and Keer[7, 8] and Luco[9].

In addition to the above studies based on integral equation techniques, an efficient semi-analytical method based on a discretization procedure has been used to solve many

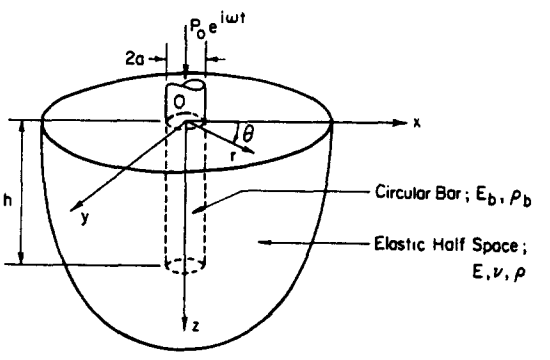

Fig. 1. Geometry of bar and embedding medium.

elastostatic load transfer problems. In this method, a homogeneous half-space subjected to unknown tractions along a fictitious contact surface is considered. The intensities of these tractions are determined by enforcing an appropriate unit rigid body displacement mode at discrete locations of the fictitious contact surface. Poulos and Davis[10], and Suriyamongkol *et al.*[11] studied the behaviour of axially loaded rigid cylinders using this method. Extensions of this method to elastic cylindrical bars are due to Butterfield and Bannerjee[12] and Poulos and Davis[13]. Recently, Selvadurai and Rajapakse[14] presented an extensive study on the discretization method and compared the solutions with those obtained through integral equation methods.

At present, studies on the dynamics of a finite cylinder embedded in an elastic half-space are rather limited. Some early attempts[15, 16] to solve the dynamic problem were based on the approximation where the surrounding medium above the base of the cylinder is treated as a system of independent elastic layers of infinitesimal thickness. A notable advancement is the study by Apsel[17], where a boundary integral equation based on the integral representation theorem[18, 19] is established to evaluate the impedance matrix of a rigid cylindrical inclusion embedded in a layered half-space. The existing solutions to the axial vibration of an elastic bar embedded in a homogeneous half-space is due to Fowler and Sinclair[20], who extended the scheme of Ref. [2] to the elastodynamic problem, and by Sen *et al.*[21], where an extension of the discretization technique[10–14] is proposed to solve the dynamic problem.

It is shown that the extension of elastostatic load transfer algorithms to the corresponding elastodynamic problems as proposed in Refs [20, 21] may lead to a solution containing a considerable error. This is due to the inability of these algorithms to properly account for the longitudinal inertia component of the bar–half-space system. The significance of the inertia of the volume in the half-space corresponding to the elastic bar is discussed in particular detail. In addition, it is found that the use of real bar density in the solution scheme as adopted in Refs [20, 21] instead of that corresponding to a fictitious bar defined as in Ref. [2] may further distort the numerical solution.

An accurate discretization procedure is suggested for the rigid bar problem through the generalization of the load transfer model of Ref. [2]. Thereafter, an efficient solution scheme based on Lagrange's equation of motion, together with the new discretization procedure, is presented to solve the title problem. Numerical results are presented to illustrate the convergence characteristics of the present scheme and the influence of bar flexibility, geometry (h/a ratio), mass density, and frequency of excitation on the axial impedance of the system.

FUNDAMENTAL SOLUTIONS

Consider a half-space region as shown in Fig. 2(a) in which (r, θ, z) is the cylindrical polar coordinate system, and the related rectangular Cartesian coordinate system (x, y, z) is such that the z-axis is normal to the free surface. It is understood that we consider harmonic vibrations, and the term $e^{i\omega t}$ (ω is the circular frequency) is suppressed in all expressions. For an isotropic linear elastic medium undergoing torsion free axisymmetric deformations the displacements can be expressed in terms of two scalar potentials, ϕ and ψ, as

$$u = \frac{\partial \phi}{\partial r} + \frac{\partial^2 \psi}{\partial r \partial z} \tag{1a}$$

$$w = \frac{\partial \phi}{\partial z} - \frac{1}{r}\frac{\partial}{\partial r}\left(r\frac{\partial \psi}{\partial r}\right) \tag{1b}$$

where u and w are the displacements in the r- and z-directions.

In view of the representation given by eqns (1a) and (1b), the equilibrium equations

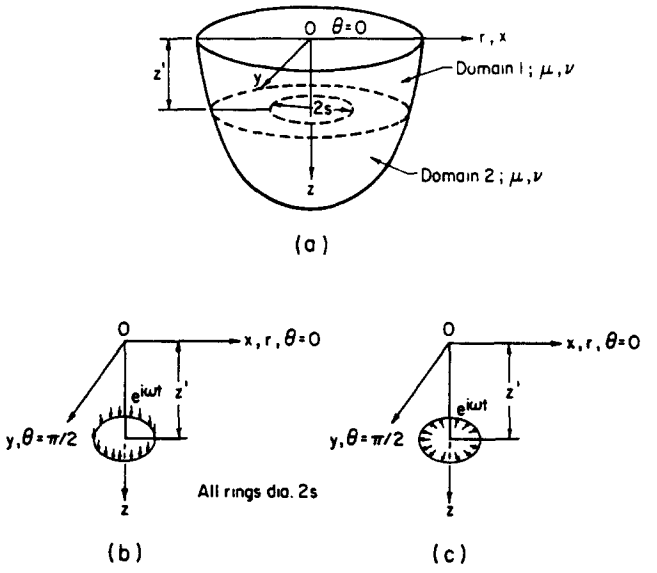

Fig. 2. Concentrated harmonic loads acting in the interior of the half-space.

for the elastic medium in the absence of body forces are satisfied provided that ϕ and ψ are the solutions to the following scalar wave equations

$$(\nabla^2 + k_p^2)\phi = 0 \tag{2a}$$

$$(\nabla^2 + k_s^2)\psi = 0 \tag{2b}$$

where $k_p^2 = \omega^2\rho/(\lambda + 2\mu)$ and $k_s^2 = \omega^2\rho/\mu$ are the pressure and shear wave numbers, respectively; λ and μ are Lame's constants; ρ the density of the medium; and ∇^2 is the axisymmetric Laplacian operator. The application of Hankel integral transforms[22] of zero-order to eqns (2a) and (2b) yields the following general solutions:

$$\phi(r,z) = \int_0^\infty \xi(A\,e^{-\alpha z} + B\,e^{\alpha z})J_0(\xi r)\,d\xi \tag{3a}$$

$$\psi(r,z) = \int_0^\infty \xi(C\,e^{-\beta z} + D\,e^{\beta z})J_0(\xi r)\,d\xi \tag{3b}$$

$$\alpha^2 = \xi^2 - k_p^2; \qquad \beta^2 = \xi^2 - k_s^2 \tag{3c}$$

where $A(\xi)$, $B(\xi)$, $C(\xi)$ and $D(\xi)$ are arbitrary functions to be determined by invoking appropriate boundary and/or continuity conditions. In view of eqns (3a) and (3b), the expressions for relevant displacements and stresses are found to be

$$w(r,z) = \int_0^\infty [\alpha(-A\,e^{-\alpha z} + B\,e^{\alpha z}) + \xi^2(C\,e^{-\beta z} + D\,e^{\beta z})]\xi J_0(\xi r)\,d\xi \tag{4a}$$

$$u(r,z) = \int_0^\infty [-(A\,e^{-\alpha z} + B\,e^{\alpha z}) - \beta(-C\,e^{-\beta z} + D\,e^{\beta z})]\xi^2 J_1(\xi r)\,d\xi \tag{4b}$$

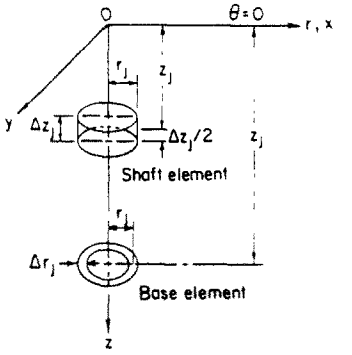

Fig. 3. Geometry of a shaft element and a base element.

$$\sigma_{zz}(r,z) = \mu \int_0^\infty [(2\xi^2 - k_s^2)(A\,e^{-\alpha z} + B\,e^{\alpha z}) + 2\beta\xi^2(-C\,e^{-\beta z} + D\,e^{\beta z})]\xi J_0(\xi r)\,d\xi \tag{4c}$$

$$\sigma_{zr}(r,z) = \mu \int_0^\infty [-2\alpha(-A\,e^{-\alpha z} + B\,e^{\alpha z}) - (2\xi^2 - k_s^2)(C\,e^{-\beta z} + D\,e^{\beta z})]\xi^2 J_1(\xi r)\,d\xi. \tag{4d}$$

Before proceeding to further analysis, it is convenient to nondimensionalize the problem by defining a length parameter "a", which denotes the radius of the embedded bar. Consider the problem of a homogeneous half-space (Fig. 2(a)) subjected to concentrated circular ring loads of unit intensity acting in the vertical and radial directions, as shown in Figs 2(b) and (c). These loads are assumed to act along the circumference of a circle, with radius equal to s at the interior of the half-space at $z = z'$. Once the displacement solutions corresponding to these loading configurations are derived, those required in the solution schemes of Refs [2, 10–14, 20, 21] could be obtained by integrating these solutions in radial or vertical directions.

Note that by taking the appropriate limit on s, the dynamic counterpart of Mindlin's solution[23] could be easily obtained from these solutions. Therefore, solutions corresponding to loading configurations shown in Figs 2(b) and (c) are of fundamental importance, and at present these do not appear explicitly in available literature. These solutions could be derived by considering two-domain problems as suggested in Refs [11, 14] for the elastostatic case. The appropriate boundary, continuity and regularity conditions and Hankel transform representation of stress jumps at $z = z'$ remains identical to those corresponding to the elastostatic problem as given in Refs [11, 14]. For brevity, these are not reproduced here. The solution of the appropriate boundary value problem yields the expressions for displacements as given by eqns (A1)–(A4) in the appendix.

In applying the discretization technique[10–14] to solve embedded cylindrical inclusions, solutions corresponding to uniformly distributed tractions of unit intensity acting on shaft and base elements shown in Fig. 3 are required. These solutions could be developed by integrating the solution given by eqns (A1)–(A4) across the thickness of the shaft and base elements. The expression for displacement in the k-direction ($k = r, z$) at point $P_i(r_i, z_i)$ due to tractions in the l-direction ($l = r, z$) acting on element j with coordinates (r_j, z_j) (see Fig. 3) is denoted by $f^{kl}(r_i, z_i; r_j, z_j)$. The explicit representation of $f^{kl}(r_i, z_i; r_j, z_j)$ for shaft and base elements are given by eqns (A13)–(A20) in the appendix.

ELASTIC CYLINDRICAL BAR EMBEDDED IN HALF-SPACE

Figure 1 shows a cylindrical elastic bar of radius a and length h ($h/a \gg 1$) partially embedded in a surrounding elastic half-space. A cylindrical coordinate system (r, θ, z) is defined such that the z-axis coincides with the longitudinal centroidal axis of the cylinder

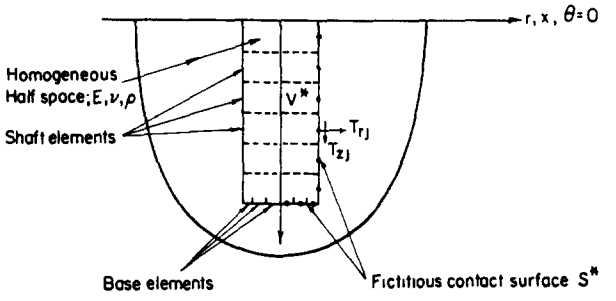

Fig. 4. Model considered in the discretization technique.

and is normal to the stress-free surface of the half-space. The material properties of the bar, which is assumed to behave as a one-dimensional elastic continuum, are characterized by its Young's modulus E_b and mass density ρ_b. The surrounding half-space is characterized by its Young's modulus, Poisson's ratio, and mass density, denoted by E, ν, and ρ, respectively. It is assumed that the bar is continuously bonded to the surrounding half-space along the shaft of the bar ($r = a$, $0 \leq \theta \leq 2\pi$, $0 \leq z \leq h$), and along the base of the bar ($z = h$, $0 \leq r \leq a$). The bar–half-space system is subjected to a symmetric harmonic axial load equivalent to $P_0 e^{i\omega t}$ at the top end of the bar at $z = 0$. It is assumed that the frequency of excitation is sufficiently low and $h/a \gg 1$, so that the use of a one-dimensional continuum model based on first-order theory is justified for the case of an elastic bar.

Before we present an accurate solution scheme for the title problem, attention is focused on solution schemes of Refs [20, 21]. In what follows, the discretization technique employed in Ref. [21] is briefly discussed through the consideration of a rigid bar problem.

In applying the discretization technique, a homogeneous half-space (without any inclusion) subjected to an unknown traction distribution along a fictitious contact surface S^*, as shown in Fig. 4, is considered. The intensities of these tractions are determined by discretizing the surface S^* using the shaft and base elements shown in Fig. 3, and establishing a flexibility equation for discrete points on S^* so as to satisfy the appropriate rigid body displacement mode. In doing so, the following simultaneous equation system is obtained

$$\sum_{j=1}^{M} [f^{zz}(r_i, z_i; r_j, z_j)T_{zj} + f^{zr}(r_i, z_i; r_j, z_j)T_{rj}] = \Delta_0 \tag{5a}$$

$$\sum_{j=1}^{M} [f^{rz}(r_i, z_i; r_j, z_j)T_{zj} + f^{rr}(r_i, z_i; r_j, z_j)T_{rj}] = 0 \qquad (i = 1, \ldots, M). \tag{5b}$$

In eqns (5a) and (5b), M is the total number of elements used to model surface S^*, Δ_0 is the specified vertical displacement along S^*, and f^{kl} are given by eqns (A13)–(A20). Intensities of radial and vertical tractions acting on the jth element are denoted by T_{rj} and T_{zj}. Solution of eqns (5a) and (5b) with $\Delta_0 = 1$ yields the numerical values for T_{rj} and T_{zj}.

It should be realized that in order to obtain a proper solution corresponding to a rigid cylinder from tractions T_{zj} resulting from eqns (5a) and (5b), due consideration must be given to the resultant longitudinal inertia force of V^*. The following relationship could be established between the magnitude of the harmonic axial force $\bar{P}_0$ corresponding to a *massless* rigid cylinder, traction resultant $R_z \left(= \sum_{j=1}^{M} T_{zj} \mathrm{d}A_j$, where $\mathrm{d}A_j$ is the surface area of the jth element$\right)$ and inertia component $I_z \left(= \int_{V^*} \rho\omega^2 w \, \mathrm{d}v \right)$ of V^*

$$\bar{P}_0 = R_z + I_z. \tag{6}$$

Figure 5 presents a comparison of non-dimensional axial impedance K_v^0 ($= \bar{P}_0/\mu a \Delta_0$)

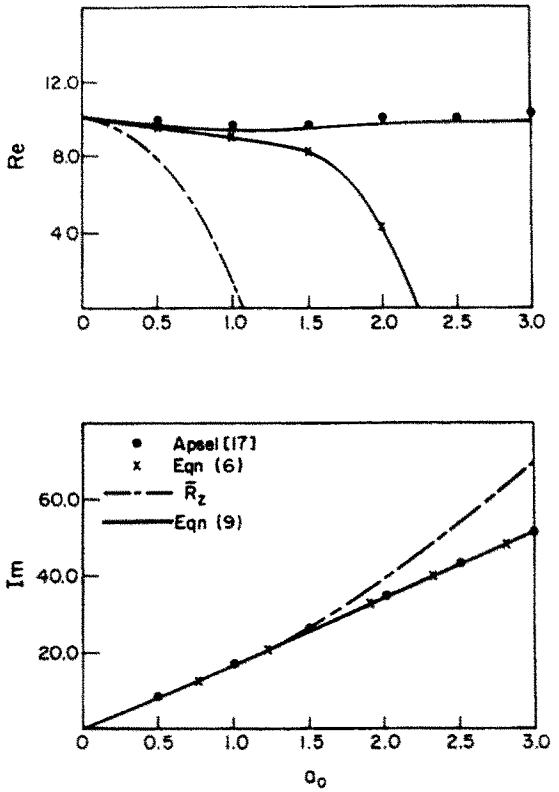

Fig. 5. Comparison of vertical impedance (K_v^0) of a massless rigid cylinder embedded in a half-space ($h/a = 2$, $\nu = 0.25$, $M = 24$ in eqns (5a) and (5b), $M_1 = 30$ and $M_2 = 10$ in eqns (9a)–(9c)).

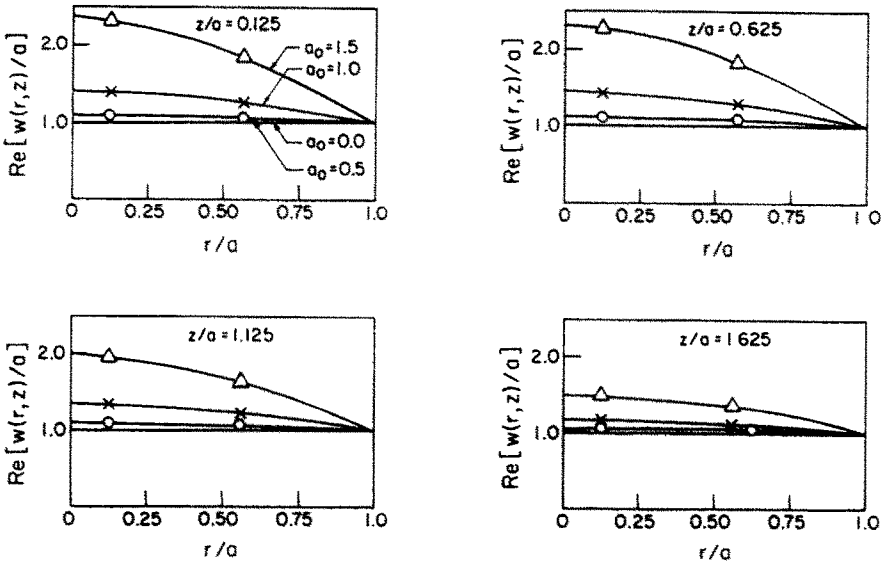

Fig. 6. Vertical displacement profiles at various z-values of domain V^* due to tractions applied on S^* ($h/a = 2.0$, $\nu = 0.25$, $M = 24$ in eqns (5a) and (5b)).

of a massless rigid cylinder obtained using eqns (5) and (6) with those due to Apsel[17]. The traction resultant R_z is also nondimensionalized as $\bar{R}_z$ ($= R_z/\mu a \Delta_0$) and plotted in Fig. 5. The displacement profiles of V^* (on the basis of which I_z is computed) due to tractions T_{zj} obtained from eqns (5a) and (5b) is presented in Fig. 6. It should be mentioned here that for $a_0 > 1.0$, where $a_0 = ak_s$, accurate computation of I_z is encountered with numerical problems and the solution scheme fails with increasing a_0.

In Ref. [21] for the case of a long elastic bar, neglecting radial tractions T_{rj} on S^*, eqns (5a) and (5b) were reduced to the form

$$\sum_{j=1}^{M} f^{zz}(r_i, z_i; r_j, z_j) T_{zj} = w_i(r_i, z_i) \tag{7a}$$

and the following governing equation was considered for the bar

$$E_b \pi a^2 \frac{d^2 w}{dz^2} + 2\pi a T_z + \pi a^2 \rho_b \omega^2 w = 0. \tag{7b}$$

Obviously, a solution based on eqns (7a) and (7b) does not properly take into account the inertia component of V^*. In addition, the use of E_b and ρ_b in eqn (7b) does not represent the proper decomposition of the bar–half-space system. Since eqn (7a) is valid *only* for an extended half-space where the domain of the elastic bar is filled with a material identical to the surrounding half-space, it is essential to consider a fictitious bar as defined by Muki and Sternberg[2]. Therefore, in eqn (7b), E_b and ρ_b should be replaced by E^* and ρ^* defined as

$$E^* = E_b - E > 0 \tag{8a}$$

$$\rho^* = \rho_b - \rho \geq 0. \tag{8b}$$

For elastostatic problems in geomechanics, usually $\bar{E} = E_b/E > 50$, hence solutions corresponding to E_b and E^* would be nearly identical. However, in all practical situations, $\rho^* \neq \rho_b$, and, as will be shown later, for elastodynamic problems, solutions would differ considerably when $a_0 > 0.25$.

It should be mentioned here that even a solution based on eqns (7a) and (7b) with E^* and ρ^* may not represent a proper solution to the title problem. This is due to the fact that as a_0 increases, displacements within V^* would differ from those along S^* and the determination of I_z on the basis of displacements along S^* may be inaccurate. In a subsequent section, this fact is verified through some representative numerical results. It is noted that the solution scheme of Ref. [20] also does not account for the longitudinal inertia component of V^*, and the decomposition of the problem on the basis of eqn (7b) would further distort the solution.

An accurate solution for the title problem should properly account for inertial forces of V^* and should take into account a fictitious bar with properly modified material parameters. In addition, the solution for an elastic bar with mass density ρ_b as $E_b \to \infty$ should yield the correct solution corresponding to a rigid bar of mass density ρ_b.

In order to develop an accurate solution scheme for the title problem, we focus our attention to the elastostatic load transfer model of Muki and Sternberg[2]. In the analysis presented in Ref. [2], an elastic half-space containing an embedded elastic bar is decomposed into an extended half-space and a fictitious bar. Initially, we apply the restriction that the bar is rigid; therefore, consideration is given only to the extended half-space as shown in Fig. 7. In order to account for the case of a short bar, it is assumed that V^* is subjected to body forces (B_r, B_z), and concentrated load transfer represented by tractions T_r, T_z acting on the terminal cross-sections at $z = 0$, h. To ensure that volume V^* deforms as a rigid body, it is assumed that the magnitude of body forces varies in both the r- and z-directions, and that the tractions vary in the r-direction.

The magnitude of body forces and tractions are determined by discretizing V^* and

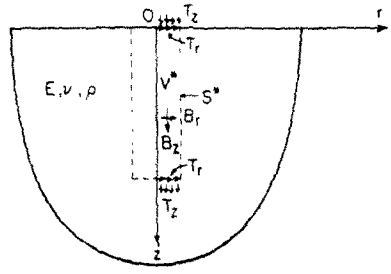

Fig. 7. Extended half-space subjected to end tractions and a body force field

terminal cross-sections using toroidal and base elements as shown in Figs 8 and 3, respectively, and establishing the following flexibility and equilibrium equations

$$\sum_{j=1}^{M_1} [\bar{f}^{zz}(r_i, z_i; r_j, z_j)B_{zj} + \bar{f}^{zr}(r_i, z_i; r_j, z_j)B_{rj}] + \sum_{j=1}^{M_2} [f^{zz}(r_i, z_i; r_j, z_j)T_{zj} + f^{zr}(r_i, z_i; r_j, z_j)T_{rj}] - \Delta_0 = 0 \quad (9a)$$

$$\sum_{j=1}^{M_1} [\bar{f}^{rz}(r_i, z_i; r_j, z_j)B_{zj} + \bar{f}^{rr}(r_i, z_i; r_j, z_j)B_{rj}] + \sum_{j=1}^{M_2} [f^{rz}(r_i, z_i; r_j, z_j)T_{zj} + f^{zr}(r_i, z_i; r_j, z_j)T_{rj}] = 0 \quad (9b)$$

$$\sum_{j=1}^{M_1} B_{zj} 2\pi r_j \Delta z_j \Delta r_j + \sum_{j=1}^{M_2} T_{zj} 2\pi r_j \Delta r_j + (\rho - \rho_b)\pi a^2 \omega^2 h \Delta_0 = P_0. \quad (9c)$$

In eqns (9a)–(9c), M_1 is the number of toroidal elements used to model V^*, M_2 is the number of base elements, $\bar{f}^{zz}$, $\bar{f}^{rz}$, $\bar{f}^{zr}$, $\bar{f}^{rr}$ are obtained by integrating eqns (A1)–(A4) over the area of a toroidal element, B_{zj} and B_{rj} represent the magnitude of body forces acting on the jth toroidal element, T_{zj} and T_{rj} are the magnitude of tractions acting on the jth base element.

Solutions of eqns (9a)–(9c) results in B_{zj}, B_{rj}, T_{zj}, T_{rj}, and Δ_0 for a given P_0. In order to compare solutions with Apsel[17], eqns (9a)–(9c) are solved with $\rho_b = 0$ and $P_0 = 1$. The axial impedance $K_v^0 (= P_0/\mu a \Delta_0)$ so obtained is plotted in Fig. 5. It is evident that this model could be used effectively to determine the impedance of a rigid cylinder. In solving eqns (9a)–(9c), it is found that better numerical convergence and efficiency is achieved by placing the displacement compatibility points (r_i, z_i) along the outer edge of an element. Note that solution of eqns (9a)–(9c) with $\rho = \rho_b$ would eliminate the inertia term in eqn (9c). Therefore, solution of eqns (9a) and (9b) for a given Δ_0 could be considered as the solution corresponding to a bar with density identical to the surrounding half-space. With this observation, we focus our attention to the title problem and present an accurate

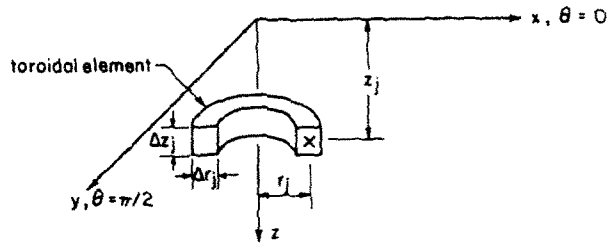

Fig. 8. Geometry of toroidal element.

solution scheme which is based on Lagrange's equations of motion and a simplified version of eqns (9a)–(9c).

In the case of the system shown in Fig. 1, a fictitious bar with material properties as defined in eqns (8a) and (8b) has to be considered in addition to the extended half-space. The deformation of the fictitious bar (identical to that of a real bar), which is assumed to behave as a one-dimensional elastic continuum, is approximated in the following form:

$$w(z,t) = \sum_{n=1}^{N} a_n(t)\,e^{-(n-1)z/h} \tag{10a}$$

$$\dot{w}(z,t) = \sum_{n=1}^{N} \dot{a}_n(t)\,e^{-(n-1)z/h} \tag{10b}$$

where $a_1,\ldots,a_N$ can be viewed as generalized coordinates. From eqns (10a) and (10b) the strain and kinetic energies U_a and T_a of the fictitious bar can be expressed as

$$U_a = \sum_{m=1}^{N}\sum_{n=1}^{N} D_{mn}a_m a_n \tag{11}$$

$$T_a = \sum_{m=1}^{N}\sum_{n=1}^{N} C_{mn}\dot{a}_m\dot{a}_n \tag{12}$$

where

$$D_{mn} = \frac{\pi E^* a^2(n-1)(m-1)(1-e^{-(m+n-2)})}{2(m+n-2)h}, \qquad m+n \neq 2$$
$$= 0, \qquad m+n=2 \tag{13}$$

$$C_{mn} = \frac{\pi\rho^* h a^2(1-e^{-(m+n-2)})}{2(m+n-2)}, \qquad m+n \neq 2$$
$$= \frac{\pi\rho^* h a^2}{2}, \qquad m+n=2 \tag{14}$$

and the superscript dot denotes differentiation with respect to time.

In the case of a long elastic bar, it is reasonable to neglect body force and traction in the r-direction. Consider the extended half-space, which is subjected to an unknown body force distribution (B_z) in V^*, and vertical traction (T_z) on circular areas at $z=0$ and h which produce the same displacement distribution as eqn (10a) in V^*. Since the body force, B_z, and the traction T_z, cannot be obtained analytically, a numerical solution is sought using the proposed discretization technique. By discretizing the volume V^* using toroidal elements and the terminal cross-sections by using base elements, we establish the following flexibility equation:

$$[A_{ij}^1 \,\vdots\, A_{ij}^2]\begin{bmatrix} B_z \\ \cdots \\ T_z \end{bmatrix} = [w^1 \,\vdots\, w^2 \,\vdots\, w^N]_{M\times N} \tag{15}$$

where

$$[A_{ij}^1]_{M\times M_1} = [f^{zz}(r_i, z_i; r_j, z_j)] \tag{16a}$$

$$[A_{ij}^2]_{M\times M_2} = [f^{zz}(r_i, z_i; r_j, z_j)] \tag{16b}$$

$$\{w^n\} = \langle e^{-(n-1)z_1/h} \ldots e^{-(n-1)z_i/h} \ldots e^{-(n-1)z_M/h}\rangle^T \tag{17}$$

$$[B_z]_{M_1 \times N} = [B_z^1 \;\vdots\; \vdots \;\vdots\; B_z^N] \tag{18a}$$

$$[T_z]_{M_2 \times N} = [T_z^1 \;\vdots\; \vdots \;\vdots\; T_z^N] \tag{18b}$$

$$\{B_z^n\} = \{B_{zj}^n\}_{M_1 \times 1} \tag{18c}$$

$$\{T_z^n\} = \{T_{zj}^n\}_{M_2 \times 1} \tag{18d}$$

and $M = M_1 + M_2$.

In eqns (15)–(18), M_1 is the number of toroidal elements used to model V^*, M_2 is the number of base elements, f^{zz} is given by eqn (A17), and $\bar{f}^{zz}$ is as defined in eqns (9a)–(9c). The intensity of the body force acting on the jth toroidal element is denoted by B_{zj}^n and T_{zj}^n is the intensity of the vertical traction on the jth base element. $\{w^n\}$ consists of vertical displacements corresponding to the nth term of eqn (10a) when $a_n = 1$. The solution of eqn (15) yields the elements of matrices $[B_z]$ and $[T_z]$. The body force B_{zj} and traction T_{zj} corresponding to the displacement given by eqn (10a) can be written as

$$B_{zj} = \sum_{n=1}^{N} a_n B_{zj}^n \qquad (j = 1, \ldots, M_1) \tag{19}$$

$$T_{zj} = \sum_{n=1}^{N} a_n T_{zj}^n \qquad (j = 1, \ldots, M_2). \tag{20}$$

Let us consider the strain and kinetic energies of the extended half-space. Introducing standard indicial notation and using the identity

$$1/2 \int_V \sigma_{ij}\varepsilon_{ij}\,dv = 1/2 \int_S u_i T_i\,ds + 1/2 \int_V u_i B_i\,dv - 1/2 \int_V \rho\, u_i \ddot{u}_i\,dv \tag{21}$$

the Lagrangian[24] for the extended half-space can be written as

$$L_h = \tfrac{1}{2}\frac{\partial}{\partial t}\int_V \rho u_i \dot{u}_i\,dv - \tfrac{1}{2}\int_{S_1} u_i T_i\,ds - \tfrac{1}{2}\int_{S_2} u_i T_i\,ds - \tfrac{1}{2}\int_{V^*} u_i B_i\,dv. \tag{22}$$

In eqn (22) V denotes the volume of the extended half-space and S_1 and S_2 are the area of terminal cross-sections at $z = 0$ and h, respectively, in the extended half-space. Note that displacement, velocity, tractions and body forces in V can be expressed in terms of the generalized coordinates.

The application of Lagrange's equation of motion[24] to the total system, composed of an extended half-space and a fictitious bar, together with eqns (10)–(22) results in the following algebraic equations of motion for a_n's

$$\sum_{n=1}^{N} a_n \Bigg[-2\omega^2 C_{ni} + 2D_{ni} + \pi \sum_{j=1}^{M_2} r_j (T_{zj}^i E_{nj} + T_{zj}^n E_{ij}) \Delta r_j + \pi \sum_{j=1}^{M_1} r_j (B_{zj}^i E_{nj} + B_{zj}^n E_{ij}) \Delta z_j \Delta r_j \Bigg] = P_0 \tag{23a}$$

$$(i = 1, 2, \ldots, n)$$

where

$$E_{nj} = e^{-(n-1)z_j/h}; E_{ij} = e^{-(i-1)z_j/h}. \tag{23b}$$

In developing eqn (23a), the integrals in eqn (22) were numerically evaluated utilizing

Table 1. Dependence of K_v on the number of toroidal elements (M_1) and base elements (M_2): $h/a = 10.0$, $a_0 = 1.0$, $\bar{\rho} = 1.0$, $\nu = 0.25$, $N = 8$

	$K_v = P_0/\mu a \Delta_0$	
(M_1, M_2)	$\bar{E} = 100$	$\bar{E} = 500$
(20, 4)	(17.10, 60.25)	(4.14, 66.10)
(40, 4)	(17.74, 60.75)	(4.39, 69.03)
(60, 6)	(17.79, 61.02)	(4.46, 69.61)
(80, 8)	(17.92, 61.90)	(4.50, 70.10)

toroidal and base elements. Note that the manipulation involved in deriving eqn (23a) is identical to that in a finite element formulation of an elastodynamic problem[25]. After solving eqn (23a), the vertical displacement at the top end of the bar is obtained from

$$\Delta_0 = \sum_{n=1}^{N} a_n. \tag{24}$$

As an alternative to the function bases given by eqn (10a), a polynomial variation of the following form could be used to approximate the vertical displacement of the bar

$$w(z,t) = \sum_{n=1}^{N} a_n(t)(z/h)^{n-1}. \tag{25}$$

With the above representation, the equations of motion of the system remain identical to eqn (23a) except that P_0 on the right-hand side of eqn (23a) is replaced by $P_0\delta_{1i}$, where δ_{ij} is Kronecker's delta function, and quantities C_{ni}, D_{ni}, E_{nj} and E_{ij} are defined as

$$C_{ni} = \frac{\pi a^2 \rho^* h}{2(n+i-1)} \tag{26a}$$

$$D_{ni} = \frac{\pi a^2 E^*(n-1)(i-1)}{2h(n+i-3)} \qquad \text{for } n+i \neq 3$$
$$= 0 \qquad \text{for } n+i = 3 \tag{26b}$$

$$E_{nj} = (z_j/h)^{n-1}; E_{ij} = (z_j/h)^{i-1}. \tag{26c}$$

A comparison on the performance of both exponential and polynomial approximations is presented in the subsequent section.

DISCUSSION AND CONCLUSIONS

A numerical study is performed initially by varying the number of elements (M_1, M_2) used to model V^* and the number of terms (N) used in displacement approximations given by eqns (10a) and (25) to determine the convergence of the proposed solution scheme. Table 1 presents a study on the dependence of a number of toroidal elements (M_1) and base elements (M_2) on the axial impedance K_v ($K_v = P_0/\mu a \Delta_0$) of the bar–half-space system [$h/a = 10.0$, $\bar{\rho} = 1$ ($\bar{\rho} = \rho_b/\rho$), $a_0 = 1.0$ ($a_0 = ak_s$), $\nu = 0.25$, $N = 8$] for a flexibility ratio $\bar{E} = 100$ and 500, where $\bar{E} = E_b/E$. It is noted that solutions are converging and the

Table 2. Comparison of convergence of K_v obtained from different displacement functions. $h/a = 10.0$, $\bar{E} = 10.0$, $\bar{\rho} = 1.0$, $\nu = 0.25$, $M_1 = 80$, $M_2 = 8$

N	$K_v = P_0/\pi a u_0$			
	$a_0 = 0.4$		$a_0 = 1.0$	
	Exponential	Polynomial	Exponential	Polynomial
1	(24.82, 33.10)	(24.82, 33.10)	(0.51, 72.61)	(0.51, 72.61)
2	(14.10, 9.20)	(15.12, 11.23)	(12.62, 18.12)	(12.61, 18.10)
4	(14.42, 8.42)	(14.31, 8.51)	(16.04, 16.62)	(16.01, 16.60)
6	(14.35, 8.40)	(14.35, 8.41)	(16.04, 16.62)	(16.04, 16.62)
8	(14.35, 8.40)	(14.35, 8.40)	(16.04, 16.62)	(16.04, 16.62)
10	(14.35, 8.40)	(14.35, 8.40)	(16.04, 16.62)	(16.04, 16.62)

algorithm is stable for varying M_1 and M_2. In view of high computational cost, it is reasonable to use $M_1 = 40$ and $M_2 = 4$ for a bar with $h/a = 10.0$. Table 2 presents a comparison of axial impedance of an elastic bar–half-space system [$h/a = 10.0$, $\bar{E} = 10.0$, $\bar{\rho} = 1, \nu = 0.25, M_1 = 80, M_2 = 8$] obtained by using different N values for both exponential and polynomial type displacement approximations for the bar. It is evident that both function bases converge rapidly in the non-dimensionalized frequency range $a_0 = 0$–1.0 and a stable solution could be obtained by using only six terms ($N = 6$).

Table 3 presents a comparison of the axial impedance of an elastic bar–half-space system obtained on the basis of both exponential and polynomial approximations for different values of $\bar{E}$ at $a_0 = 0.4$ and 1.0. Both function bases yield solutions which agree very closely. These studies confirm the overall convergence and validity of the present solution scheme for different problem configurations. In all numerical solutions, volume V^* and terminal cross-sections are subdivided using equal spacing in a particular direction. It should be mentioned here that the axial impedance obtained by neglecting tractions on terminal cross-sections (i.e. $T_{zj} = 0$ at $z = 0$, h and solving eqn (15) only for B_{zj}) hardly shows any difference.

Figures 9–11 illustrate the influence of flexibility ratio $\bar{E}$ and non-dimensionalized frequency parameter a_0 on the axial impedance of an elastic bar–half-space system for $h/a = 5$, 10 and 15, respectively. It appears from these figures that within a certain range of $\bar{E}$, the real part of axial impedance shows an increase with increasing a_0. As $\bar{E}$ increases beyond this range, the real part of axial impedance decreases rapidly with increasing a_0 reflecting a behaviour similar to that of a rigid bar of mass density ρ_b embedded in a half-space. Note that as the bar becomes rigid, the inertia components dominate and the solution shows a great dependence on the frequency of excitation. The imaginary part of the axial impedance in the range $a_0 = 0$–1.0 shows nearly linear dependence on a_0 for all values of $\bar{E}$ (flexible as well as rigid). In Figs 9–11, axial impedance of a rigid bar ($\bar{E} = \infty$) obtained by using eqns (9a) and (9b) with B_{rj}, $T_{rj} = 0$ is also plotted. It can easily be seen that the results obtained from the variational solution scheme presented for an elastic bar approach the curves corresponding to $\bar{E} = \infty$ as the value of $\bar{E}$ is increased.

Table 3. Comparison of K_v obtained from exponential and polynomial function bases for different $\bar{E}$, $h/a = 10.0$, $\bar{\rho} = 1.0$, $\nu = 0.25$, $N = 6$, $M_1 = 80$, $M_2 = 8$

$\bar{E}$	$K_v = P_0/\pi a u_0$			
	$a_0 = 0.40$		$a_0 = 1.0$	
	Exponential	Polynomial	Exponential	Polynomial
10	(14.35, 8.40)	(14.35, 8.40)	(16.04, 16.62)	(16.04, 16.62)
50	(23.16, 21.31)	(23.17, 21.29)	(25.82, 49.14)	(25.61, 49.15)
100	(24.06, 25.60)	(24.07, 25.60)	(17.92, 61.90)	(17.94, 61.90)
500	(24.91, 31.61)	(24.92, 31.60)	(4.50, 70.10)	(4.51, 70.11)
1000	(24.31, 32.81)	(24.33, 32.80)	(2.61, 71.31)	(2.61, 71.33)

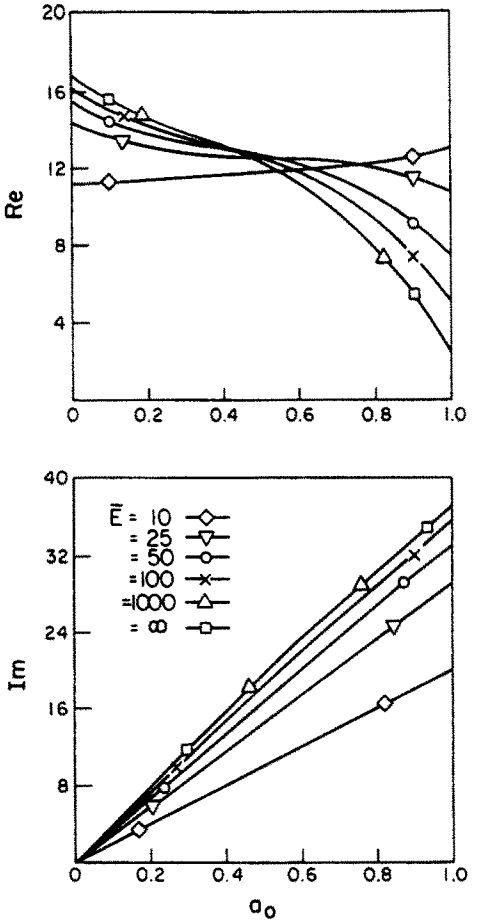

Fig. 9. Variation of vertical impedance, K_v, of a cylindrical elastic bar for various $\bar{E}(h/a = 5.0, \nu = 0.25, \bar{\rho} = 1.0, M_1 = 20, M_2 = 4)$.

Figure 12 illustrates the influence of mass density ratio $\bar{\rho}(\bar{\rho} = \rho_b/\rho)$ on the axial impedance of an elastic bar ($h/a = 10.0$, $\bar{E} = 100.0$) in the frequency range $a_0 = 0$–1.0. These results show that the axial impedance has marked dependence on the mass density ratio $\bar{\rho}$ of the elastic bar–half-space system when $a_0 > 0.25$. Figure 12 can be used to show the effect of using ρ_b instead of ρ^* in the solution as considered in Refs [20, 21]. Consider a bar where $\rho_b = \rho$, then $\bar{\rho} = 1$ and $\rho^* = 0$. The appropriate solution is given by the curve corresponding to $\bar{\rho} = 1$ in Fig. 12. If we use ρ_b in eqn (7b) as suggested in Refs [20, 21] which is equivalent to considering a fictitious bar with $\rho^* = \rho_b$, then the solution obtained would be identical to that in Fig. 12 corresponding to $\bar{\rho} = 2$. The differences between impedances given by curves corresponding to $\bar{\rho} = 1$ and 2 could be easily seen in Fig. 12. Furthermore, the use of ρ_b instead of ρ^* would never make the solution approach the correct limit of a rigid bar with a mass density ρ_b as $\bar{E} \to \infty$.

At this stage, attention is focused on the load transfer model which is based on tractions applied only on fictitious contact surface S^*. If we solve the elastic bar problem by applying the variational scheme and *taking the modified value for mass density* (ρ^*), then the following equations of motion are obtained to determine a_n

$$\sum_{n=1}^{N} a_n \left[-2\omega^2 C_{ni} + 2D_{ni} + \pi \sum_{j=1}^{M} r_j (T^i_{zj} E_{nj} + T^n_{zj} E_{ij}) \Delta t_j \right] = P_0$$

$$(i = 1, \ldots, N). \tag{27}$$

In eqn (27), M is the total number of shaft and base elements used to model S^* and Δt_j

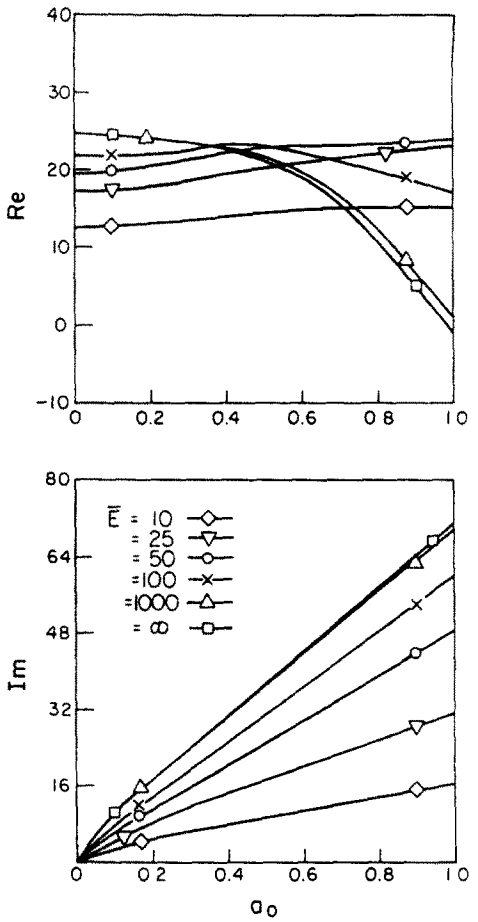

Fig. 10. Variation of vertical impedance, K_v, of a cylindrical elastic bar for various $\bar{E}$ (h/a = 10.0, ν = 0.25, $\bar{\rho}$ = 1.0, M_1 = 40, M_2 = 4).

denotes Δz_j or Δr_j. In eqn (27) T^n_{zj} is obtained by solving the following flexibility equation established for surface S^*

$$[F]\{T^n_{zj}\} = \{w^n\} \qquad (n = 1, \ldots, N). \tag{28}$$

The elements of $[F]$ are given by eqns (A13) and (A17).

For the purposes of identification, solutions obtained from eqn (23a) are referred to as Scheme 1 solutions and those from eqn (27) as Scheme 2 solutions. Table 4 presents a comparison of axial impedance obtained from Schemes 1 and 2 for an elastic bar (h/a = 10.0, $\bar{\rho}$ = 1.0, ν = 0.25) for different $\bar{E}$ and a_0 values. For a_0 = 0.4, the solutions agree very closely, and increasing differences are observed as a_0 increases. Especially for a_0 = 1.5, the solutions obtained from Schemes 1 and 2 show very large differences. The reason for the failure of solutions obtained from eqn (27) is that as a_0 increases, it is incorrect to assume that displacement in V^* due to tractions on S^* is uniform within $0 \leqq r \leqq a$ (see also Fig. 6). The inability of the algorithm to properly account for inertia of V^* or to impose uniform displacement within $0 \leqq r \leqq a$ leads to distorted solutions.

The present formulation could also be used to determine the applicability of a load transfer model where it is assumed that the body force in V^* and tractions in the terminal cross-sections are distributed uniformly in the radial direction. In this case, eqn (23a) is solved with a single toroidal element in the r-direction. Since vertical displacement is not uniform in the radial direction within V^*, compatibility between the extended half-space and the fictitious bar can be imposed on any location in V^* with $0 \leqq r \leqq a$. Table 5

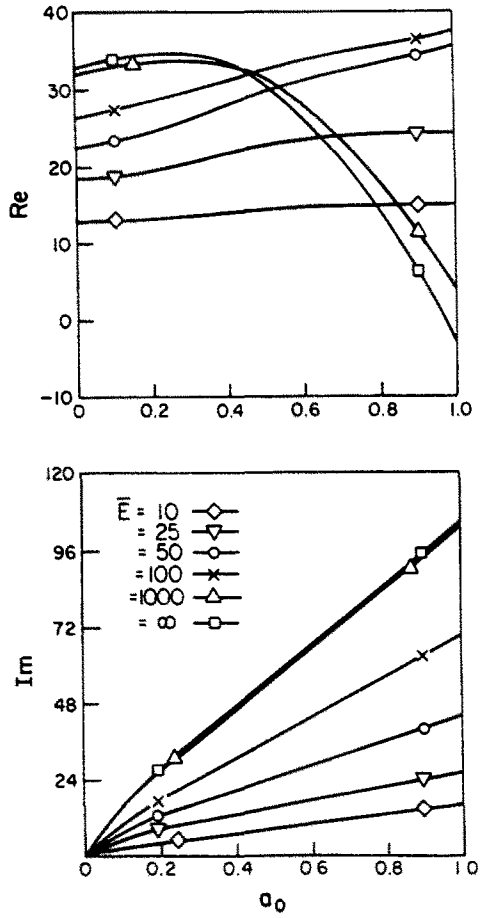

Fig. 11. Variation of axial impedance, K_v, of a cylindrical elastic bar for various $\bar{E}$ ($h/a = 15$, $\nu = 0.25$, $\bar{\rho} = 1.0$, $M_1 = 60$, $M_2 = 6$).

presents axial impedance of a bar–elastic half-space system ($h/a = 10.0$, $\nu = 0.25$, $\bar{\rho} = 1.0$) obtained using this model with displacement compatibility imposed in V^* at $r = 0$ (along z-axis) and $r = a$ (along the fictitious contact surface S^*). It is observed that solutions based on compatibility along S^* (i.e. $r = a$) agree very closely with the non-uniform body force model when a_0 is sufficiently small, preferably $a_0 \leqq 0.5$. Solutions based on displacement compatibility along the z-axis are found to deviate considerably, even at low frequencies.

Based on the above comprehensive investigation, the following conclusions could be made.

(a) The present solution scheme, based on Lagrange's equation of motion and the discretization technique, solves the title problem over a wide range of frequencies.

(b) The use of real bar density (ρ_b) in the solution procedure instead of that corresponding to the fictitious bar ($\rho^* = \rho_b - \rho$) is shown to produce a considerable error on the axial impedance of the system when $a_0 > 0.25$.

(c) The solution algorithm such as those based on tractions and displacement compatibility along the fictitious contact surface S^* or the uniform body force model with displacement compatibility along S^* could be considered as accurate and numerically efficient if $a_0 \leqq 0.5$. In these solutions, it is essential to use a fictitious bar with material properties as defined in eqns (8a) and (8b).

(d) As for limitations of the present schemes, $h/a \gg 1$ and the frequency of excitation should be such that the one-dimensional behaviour of the bar is justifiable and the displacement of the bar could be approximated by eqns (10) or eqn (25) with a reasonable

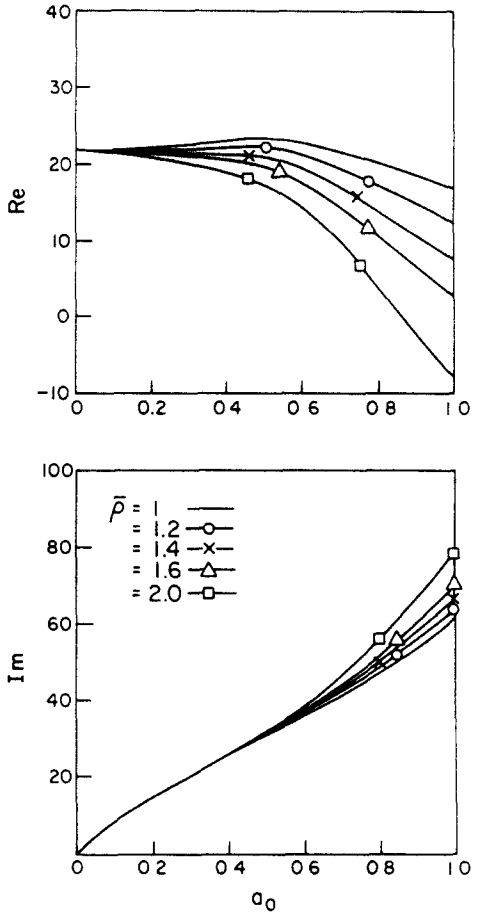

Fig. 12. Variation of axial impedance, K_v, for different density ratios ($h/a = 10.0$, $\nu = 0.25$, $\bar{E} = 100$, $M_1 = 40$, $M_2 = 4$).

Table 4. Comparison of K_v obtained from Schemes 1 and 2: $h/a = 10$, $\bar{\rho} = 1$, $\nu = 0.25$, $M_1 = 80$ and $M_2 = 8$ for Scheme 1, $M = 24$ for Scheme 2

$\bar{E}$	$K_v = P_0/\mu a \Delta_0$					
	$a_0 = 0.4$		$a_0 = 1.0$		$a_0 = 1.5$	
	Scheme 1	Scheme 2	Scheme 1	Scheme 2	Scheme 1	Scheme 2
10	(14.35, 8.40)	(14.01, 7.94)	(16.04, 16.62)	(14.68, 16.72)	(15.01, 24.06)	(10.78, 28.79)
50	(23.16, 21.31)	(22.60, 20.40)	(25.82, 49.14)	(23.15, 50.34)	(35.39, 74.21)	(35.37, 89.20)
100	(24.06, 25.00)	(23.96, 25.43)	(17.92, 61.90)	(14.01, 63.55)	(13.04, 104.42)	(-6.56, 131.80)
1000	(24.31, 32.81)	(24.42, 31.90)	(2.61, 71.31)	(-3.11, 70.81)	(-34.91, 107.2)	(-68.90, 107.30)

number of terms. For the case of a rigid or nearly rigid bar, the discretization scheme is applicable over a wide range of frequencies. However, the solution may be considerably expensive if $a_0 > 1.5$.

A natural extension of the present scheme is to study the lateral vibrations of an elastic bar embedded in a half-space and subjected to a harmonic lateral load and a moment. A companion paper presents a comprehensive study on this problem.

Acknowledgement—The work presented here was supported by grant A-7988 from the Natural Science and Engineering Research Council of Canada. We are greatly indebted to a referee whose meticulous review suggested improvements in the structure of the manuscript and investigation of some additional aspects of the problem.

Table 5. Comparison of K_v obtained using uniform and non-uniform body force model: $h/a = 10.0$, $\bar{\rho} = 1.0$, $\nu = 0.25$, $M_1 = 20$, $M_2 = 2$ (uniform body force model), $M_1 = 80$, $M_2 = 8$ (non-uniform body force model)

$\bar{E}$	$K_v = P_0/\mu a \Delta_0$					
	$a_0 = 0.4$			$a_0 = 1.0$		
	Uni. body force Displ. comp. along z-axis	Uni. body force Displ. comp. along S*	Non-uniform body force model	Uni. body force Displ. comp. along z-axis	Uni. body force Displ. Comp. along S*	Non-uniform body force model
10	(12.57, 5.78)	(13.99, 7.97)	(14.35, 8.40)	(13.90, 10.54)	(13.67, 15.55)	(16.04, 16.62)
50	(20.46, 14.33)	(22.44, 20.12)	(23.16, 21.31)	(21.50, 28.79)	(20.16, 45.94)	(25.82, 49.14)
100	(22.07, 17.38)	(23.81, 25.01)	(24.06, 25.60)	(20.20, 35.20)	(12.19, 56.69)	(17.92, 61.90)
1000	(23.49, 21.20)	(24.30, 31.40)	(24.31, 32.81)	(16.47, 41.68)	(-1.80, 62.54)	(2.61, 71.31)

REFERENCES

1. R. Muki and E. Sternberg, On the diffusion of an axial load from an infinite cylindrical bar embedded in an elastic medium. *Int. J. Solids Structures* **5**, 587 (1969).
2. R. Muki and E. Sternberg, Elastostatic load transfer to a half-space from a partially embedded axially loaded rod. *Int. J. Solids Structures* **6**, 69 (1970).
3. L. M. Keer and N. J. Freeman, Load transfer problem for an embedded shaft in torsion. *J. Appl. Mech. ASME* **37**, 959 (1970).
4. B. Niumpradit and P. Karasudhi, Load transfer from an elastic pile to a saturated porous elastic soil. *Int. J. Numer. Anal. Meth. Geomech.* **3**, 231 (1979).
5. P. Karasudhi, R. K. N. D. Rajapakse and B. Y. Hwang, Torsion of a long cylindrical elastic bar partially embedded in a layered elastic half space. *Int. J. Solids Structures* **20**, 1 (1984).
6. P. Karasudhi, R. K. N. D. Rajapakse and K. K. Liyanage, A reconsideration of elastostatic load transfer problems involving a half space. *Trans. CSME* **8**, 219 (1984).
7. V. K. Luk and L. M. Keer, Stress analysis for an elastic half space containing an axially loaded rigid cylindrical rod. *Int. J. Solids Structures* **15**, 805 (1979).
8. V. K. Luk and L. M. Keer, Stress analysis of a deep rigid axially loaded cylindrical anchor in an elastic medium. *Int. J. Numer. Anal. Meth. Geomech.* **4**, 215 (1980).
9. J. E. Luco, Torsion of a rigid cylinder embedded in an elastic half space. *J. Appl. Mech. ASME* **43**, 419 (1976).
10. H. G. Poulos and E. H. Davis, The settlement behaviour of a single axially loaded incompressible piles and piers. *Geotechnique* **18**, 351 (1968).
11. S. Suriyamongkol, P. Karasudhi and S. L. Lee, Axially loaded rigid cylindrical body embedded in a half space. *Proc. 13th Midwestern Mechanics Conf.*, p. 333. University of Pittsburgh (1973).
12. R. Butterfield and P. K. Bannerjee, The elastic analysis of compressible piles and pile groups. *Geotechnique* **21**, 43 (1971).
13. H. G. Poulos and E. H. Davis, *Pile Foundation Analysis and Design*. Wiley, New York (1980).
14. A. P. S. Selvadurai and R. K. N. D. Rajapakse, On the load transfer from a rigid cylindrical inclusion into an elastic half space. *Int. J. Solids Structures* **21**, 1213 (1985).
15. T. Nogami and M. Novak, Soil–pile interaction in vertical vibration. *Int. J. Earthquake Engng Struct. Dyn.* **4**, 277 (1976).
16. M. Novak, Vertical vibration of floating piles. *J. Engng Mech. Div. ASCE* **103**, 153 (1977).
17. R. J. Apsel, Dynamic Green's function for layered media and application to boundary value problems. Ph.D. Dissertation, University of California, San Diego, California (1979).
18. A. C. Eringen and E. H. Suhubi, *Elastodynamics II*. Academic Press, New York (1975).
19. A. T. De Hoop, Representation theorems for the displacement in an elastic solid and their application to elastodynamic diffraction theory. Doctoral Dissertation, Tech. Hogeschole, Delft (1958).
20. G. F. Fowler and G. B. Sinclair, The longitudinal harmonic excitation of a circular bar embedded in an elastic half space. *Int. J. Solids Structures* **14**, 999 (1978).
21. R. Sen, T. G. Davis and P. K. Bannerjee, Dynamic analysis of single piles and pile groups embedded in homogeneous elastic half space. *Earthquake Engng Struct. Dyn.* **13**, 53 (1985).
22. I. N. Sneddon, *Fourier Transforms*. McGraw-Hill, New York (1951).
23. R. D. Mindlin, Force at a point in the interior of a semi-infinite solid. *Physics* **7**, 195 (1936).
24. K. Washishu, *Variational Methods in Elasticity and Plasticity*, 3rd Edn. Pergamon, Oxford (1982).
25. S. S. Rao, *The Finite Element Method in Engineering*, 1st Edn. Pergamon, Oxford (1982).

APPENDIX

The following are expressions for displacements corresponding to concentrated ring forces shown in Fig. 2. Concentrated vertical ring force (Fig. 2(b))

$$w(r,z;s,z') = \int_0^\infty \alpha R_1(\xi) F_1(\xi,z,z') s\xi J_0(\xi r) J_0(\xi s)\,d\xi \tag{A1}$$

$$u(r,z;s,z') = \int_0^\infty \alpha\beta R_1(\xi) F_2(\xi,z,z') s\xi^2 J_1(\xi r) J_0(\xi s)\,d\xi. \tag{A2}$$

Concentrated radial ring force (Fig. 2(c))

$$w(r,z;s,z') = \int_0^\infty \alpha\beta R_1(\xi)F_3(\xi,z,z')s\xi^2 J_0(\xi r)J_1(\xi s)\,d\xi \tag{A3}$$

$$u(r,z;s,z') = \int_0^\infty \beta R_1(\xi)F_4(\xi,z,z')s\xi J_1(\xi r)J_1(\xi s)\,d\xi. \tag{A4}$$

The functions F_1, F_2, F_3, F_4, and R_1 appearing in eqns (A1)–(A4) are defined as

$$F_1(\xi,z,z') = 4\alpha\beta(2\xi^2 - k_s^2)(Q_1 + Q_2) + R(\xi)(\xi^2 Q_3 - \alpha\beta Q_4) - \bar{R}(\xi)(\alpha\beta Q_5 + \xi^2 Q_6) \tag{A5}$$

$$F_2(\xi,z,z') = 4(2\xi^2 - k_s^2)(\xi^2 Q_2 + \alpha\beta Q_1) - \bar{R}(\xi)(Q_5 + Q_6) - \delta R(\xi)(Q_4 - Q_3) \tag{A6}$$

$$F_3(\xi,z,z') = 4(2\xi^2 - k_s^2)(\xi^2 Q_1 + \alpha\beta Q_2) - \bar{R}(\xi)(Q_5 + Q_6) - \delta R(\xi)(Q_4 - Q_3) \tag{A7}$$

$$F_4(\xi,z,z') = 4\alpha\beta\xi^2(2\xi^2 - k_s^2)(Q_1 + Q_2) + R(\xi)(\xi^2 Q_4 - \alpha\beta Q_3) - \bar{R}(\xi)(\xi^2 Q_5 + \alpha\beta Q_6) \tag{A8}$$

$$R_1(\xi) = \frac{1}{2\mu k_s^2 \alpha\beta R(\xi)} \tag{A9a}$$

and

$$R(\xi) = (2\xi^2 - k_s^2)^2 - 4\alpha\beta\xi^2 \tag{A9b}$$

$$\bar{R}(\xi) = (2\xi^2 - k_s^2)^2 + 4\alpha\beta\xi^2 \tag{A10}$$

$$\begin{aligned} Q_1 &= e^{-\alpha z' - \beta z}, & Q_4 &= e^{-\alpha|z-z'|} \\ Q_2 &= e^{-\alpha z - \beta z'}, & Q_5 &= e^{-\alpha(z+z')} \\ Q_3 &= e^{-\beta|z-z'|}, & Q_6 &= e^{-\beta(z+z')} \end{aligned} \tag{A11}$$

$$\begin{aligned} \delta &= -1 \quad \text{if } z < z' \\ &= \ \ 1 \quad \text{if } z > z'. \end{aligned} \tag{A12}$$

Note $\alpha^2 = \xi^2 - k_p^2$, $\beta^2 = \xi^2 - k_s^2$, and $R(\xi) = 0$ is Rayleigh's equation. The branches of α and β are taken such that both real and imaginary parts of α and β are positive along the contour of integration. This ensures that integrals in eqns (A1)–(A4) are bounded and consist of waves which are out-going.

The following are expressions for displacements corresponding to distributed tractions acting on shaft or base elements (see Fig. 3).

Uniform traction in the z-direction acting on a shaft element

$$f^{zz}(r_i,z_i;r_j,z_j) = \left[\int_0^\infty \alpha R_1(\xi)F_5(\xi,z_i,z')r_j\xi J_0(\xi r_i)J_0(\xi r_j)\,d\xi\right]_{z'=z_{j1}}^{z'=z_{j2}} \tag{A13}$$

$$f^{rz}(r_i,z_i;r_j,z_j) = \left[\int_0^\infty \alpha\beta R_1(\xi)F_6(\xi,z_i,z')r_j\xi^2 J_1(\xi r_i)J_0(\xi r_j)\,d\xi\right]_{z'=z_{j1}}^{z'=z_{j2}}. \tag{A14}$$

Uniform traction in the r-direction acting on a shaft element

$$f^{zr}(r_i,z_i;r_j,z_j) = \left[\int_0^\infty \alpha\beta R_1(\xi)F_7(\xi,z_i,z')r_j\xi^2 J_0(\xi r_i)J_1(\xi r_j)\,d\xi\right]_{z'=z_{j1}}^{z'=z_{j2}} \tag{A15}$$

$$f^{rr}(r_i,z_i;r_j,z_j) = \left[\int_0^\infty \beta R_1(\xi)F_8(\xi,z_i,z')r_j\xi J_1(\xi r_i)J_1(\xi r_j)\,d\xi\right]_{z'=z_{j1}}^{z'=z_{j2}}. \tag{A16}$$

Uniform traction in the z-direction acting on a base element

$$f^{zz}(r_i,z_i;r_j,z_j) = \left[\int_0^\infty \alpha R_1(\xi)F_1(\xi,z_i,z_j)sJ_0(\xi r_i)J_1(\xi s)\,d\xi\right]_{s'=s_{j1}}^{s'=s_{j2}} \tag{A17}$$

$$f^{rz}(r_i,z_i;r_j,z_j) = \left[\int_0^\infty \alpha\beta R_1(\xi)F_2(\xi,z_i,z_j)s\xi J_1(\xi r_i)J_1(\xi s)\,d\xi\right]_{s'=s_{j1}}^{s'=s_{j2}}. \tag{A18}$$

Linearly varying traction in the r-direction along a base element

$$f^{zr}(r_i,z_i;r_j,z_j) = \left[\int_0^\infty \alpha\beta R_1(\xi)F_3(\xi,z_i,z_j)s\xi J_0(\xi r_i)J_2(\xi s)\,d\xi\right]_{s'=s_{j1}}^{s'=s_{j2}} \tag{A19}$$

$$f^{rr}(r_i,z_i;r_j,z_j) = \left[\int_0^\infty \beta R_1(\xi)F_4(\xi,z_i,z_j)s\xi J_1(\xi r_i)J_2(\xi s)\,d\xi\right]_{s'=s_{j1}}^{s'=s_{j2}}. \tag{A20}$$

The functions F_5, F_6, F_7, and F_8 and the limits z_{j1}, z_{j2}, s_{j1} and s_{j2} appearing above are defined as

$$\alpha\beta F_5(\xi,z,z') = -4\alpha\beta\xi^2(2\xi^2 - k_s^2)(\beta Q_1 + \alpha Q_2) + \alpha R(\xi)\delta(\xi^2 Q_3 - \beta^2 Q_4) + \alpha\bar{R}(\xi)(\beta^2 Q_5 + \xi^2 Q_6) \tag{A21}$$

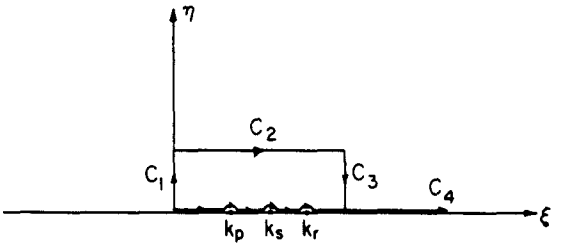

Fig. A1. Contour for numerical integration.

$$\alpha\beta F_6(\xi,z,z') = -4\alpha(2\xi^2 - k_s^2)(\xi^2 Q_2 + \beta^2 Q_1) + \bar{R}(\xi)(\beta Q_5 + \beta^2 Q_6) - R(\xi)(\beta Q_4 - \alpha Q_3) \tag{A22}$$

$$\alpha\beta F_7(\xi,z,z') = -4\beta(2\xi^2 - k_s^2)(\xi^2 Q_1 + \alpha^2 Q_2) - \bar{R}(\xi)(\beta Q_5 + \alpha Q_6) - R(\xi)(\beta Q_4 - \alpha Q_3) \tag{A23}$$

$$\alpha\beta F_8(\xi,z,z') = -4\alpha\beta\xi^2(2\xi^2 - k_s^2)(\beta Q_1 + \alpha Q_2) + \beta R(\xi)\delta(\xi^2 Q_4 - \alpha^2 Q_3) + \beta\bar{R}(\xi)(\xi^2 Q_5 + \alpha^2 Q_6) \tag{A24}$$

$$z_{j1} = z_j - \Delta z_j/2, \qquad z_{j2} = z_j + \Delta z_j/2 \tag{A25}$$

$$s_{j1} = r_j - \Delta r_j/2, \qquad s_{j2} = r_j + \Delta r_j/2. \tag{A26}$$

The evaluation of $f^{kl}(r_i, z_i; r_j, z_j)$ which consists of infinite integrals has to be done through a numerical integration scheme. For $a_0 > 0$, f^{kl} are complex and the integrands are singular at points $\xi = k_s$, k_p, and k_r where k_r is the root of Rayleigh's equation. In our opinion, an efficient way to evaluate these integrals is to perform the numerical integration along a contour taken in the first quadrant of a complex plane (ξ, η) as shown in Fig. A1.